

The Theory and Simulation of the 21-cm Background from the Epoch of Reionization

Paul R. Shapiro^{*}, Ilian T. Iliev[†], Garrelt Mellema^{**}, Ue-Li Pen[‡] and Hugh Merz[§]

^{*}*Department of Astronomy, University of Texas, Austin, TX 78712-1083, U.S.A.*

[†]*Institute of Theoretical Physics, University Zurich, Winterthurerstrasse 190, CH-8057 Zurich, Switzerland*

^{**}*Stockholm Observatory, AlbaNova University Center, Stockholm University, SE-106 91 Stockholm, Sweden*

[‡]*Canadian Institute for Theoretical Astrophysics, University of Toronto, 60 St. George Street, Toronto, ON M5S 3H8, Canada*

[§]*Department of Physics & Astronomy, University of Waterloo, 200 University Avenue West, Waterloo, ON N2L 3G1, Canada*

Abstract. The redshifted 21-cm line of distant neutral H atoms provides a probe of the cosmic “dark ages” and the epoch of reionization (“EOR”) which ended them, within the first billion years of cosmic time. The radio continuum produced by this redshifted line can be seen in absorption or emission against the cosmic microwave background (“CMB”) at meterwaves, yielding information about the thermal and ionization history of the universe and the primordial density perturbation spectrum that led to galaxy and large-scale structure formation. Observing this 21-cm background is a great challenge, as it is necessary to detect a diffuse signal at a brightness temperature that differs from that of the CMB at millikelvin levels and distinguish this from foreground continuum sources. A new generation of low-frequency radio arrays is currently under development to search for this background. Accurate theoretical predictions of the spectrum and anisotropy of this background, necessary to guide and interpret future observations, are also quite challenging. Toward this end, it is necessary to model the inhomogeneous reionization of the intergalactic medium and determine the spin temperature of the 21-cm transition and its variations in time and space as it decouples from the temperature of the CMB. In my talk, I summarized some of the theoretical progress in this area. Here, I will focus on just a few of the predictions for the 21-cm background from the EOR, based on our newest, large-scale simulations of patchy reionization. These simulations are the first with enough N-body particles (from 5 to 29 billion) and radiative transfer rays to resolve the formation of and trace the ionizing radiation from each of the millions of dwarf galaxies believed responsible for reionization, down to $10^8 M_\odot$, in a cubic volume large enough (90 and 163 comoving Mpc on a side) to make meaningful statistical predictions of the fluctuating 21-cm background.

Keywords: cosmology:theory—diffuse radiation—large-scale structure of Universe— high-redshift—galaxies: formation—intergalactic medium— radiative transfer— methods: numerical

PACS: 98.80.-k, 98.70.Vc, 95.30.Jx, 98.85Bh

INTRODUCTION

The redshifted 21-cm line of neutral hydrogen atoms can probe the thermal and ionization history of the universe from the cosmic “dark ages” through the EOR and the density perturbations responsible for structure formation (see, e.g., [1] for review and refs). It is generally believed that, during the EOR, the spin temperature, T_s , of this hyperfine transition was decoupled from the CMB temperature, T_{CMB} , by the Wouthuysen-Field

mechanism, whereby UV photons at the Ly α transition frequency are resonantly scattered, and the excited atoms then decay to a different hyperfine level of the ground state. This radiative pumping drives T_s toward the gas kinetic temperature, T_K . The 21-cm line is seen in emission or absorption against the CMB if T_s is greater than or less than T_{CMB} , respectively. If, as is also generally believed, other radiation is also present (e.g. X-rays) to heat the neutral IGM so that $T_K \gg T_{\text{CMB}}$, then the 21-cm differential brightness temperature depends only upon the neutral gas density and peculiar velocity fields, independent of the value of T_K or T_s . Henceforth, we shall limit our discussion of the 21-cm background from the EOR to this regime.

Reionization is generally believed to be the outcome of the release of ionizing radiation by galaxies undergoing star formation (see, e.g., [2, 3] for recent reviews). Current theory suggests that the galaxies responsible for most of this radiation are dwarf galaxies more massive than about $10^8 M_\odot$. While dark matter dominates the gravitational forces which cause this structure formation, ordinary atomic matter must join the dark matter in making galaxies for star formation to be possible. Once the atomic gas in the intergalactic medium (“IGM”) in some region is heated by reionization, however, gas pressure opposes gravitational collapse, and, thereafter, the smallest galaxies form without atomic matter and cannot make stars. The minimum mass of star-forming galaxies in such regions is about 10^9 solar masses. This suppression of star-forming galaxies of lower mass inside ionized regions is sometimes referred to as “Jeans-mass filtering” [4].

Due to its complexity, reionization is best studied through large-scale numerical simulations [5, 6, 7, 8], combining the numerical challenges of N -body simulation and radiative transfer. The tiny galaxies which are the dominant contributors of ionizing radiation must be resolved in very large cosmological volumes, large enough to contain billions of times more total mass than one dwarf galaxy and up to tens of millions of such galaxies, in order to derive their numbers and clustering properties correctly. The expansion of the intergalactic ionization fronts created by all these millions of galaxies must, in turn, be tracked with a 3D radiative transfer method which also solves non-equilibrium ionization rate equations. The combination of all these requirements makes this problem formidable.

Our original simulations [5] resolved the formation of all galaxies more massive than about one billion solar masses, those which are expected to form stars even after reionization has heated their environment. These simulations of a comoving, cosmologically-expanding cubic volume $(150 \text{ Mpc})^3$ enabled us to make the first statistically meaningful predictions of the impact of reionization on observables like the 21-cm background [9], the CMB anisotropy [10], and the observability of early galaxies as Lyman α line-emission sources [11], essential predictions to guide and interpret current and future observational programs [12]. With the next generation of simulations described here, we shall explore the role of less massive dwarf galaxies. These are important sources of ionizing radiation if they form before their neighborhood is reionized but are prevented from being sources if they form after it is reionized. Our previous results showed that the inclusion of these sources and of their suppression changes the outcome of reionization substantially [13]. Simulations of volume $(50 \text{ Mpc})^3$ showed that reionization was “self-regulated,” i.e. the more abundant low-mass halos initially dominated but later choked themselves off as their formation was suppressed in ionized regions. The next step, described here, is to push these simulations of “self-regulated” reionization to

larger volumes, large-enough to make meaningful statistical predictions of observables like the 21-cm background.

NEW, LARGE-SCALE SIMULATIONS OF SELF-REGULATED REIONIZATION

We have developed a new, cosmological N -body code more powerful than the one we used for our previous simulations [14]. CubeP³M, a massively-parallel P³M (particle-particle-mesh) [15] code, is a successor to the previous code, PMFAST [16]. Its force resolution is significantly better than that of PMFAST, by inclusion of the short-range correction from direct particle-particle (PP) forces. With this improved force resolution, dark matter halos can be identified with as few as 20 particles per halo, to locate all the galaxies which are possible sources of ionizing starlight, with masses above this minimum.

These N -body results provide the evolving density field of the IGM and the location and mass of all the halo sources, as input to a separate radiative transfer simulation of inhomogeneous reionization. The latter simulation is performed by our C²Ray (Conservative, Causal **R**ay-Tracing) code, a grid-based, ray-tracing, radiative transfer and nonequilibrium chemistry code, described in [17]. The ionizing radiation is ray-traced from every source to every grid cell using a method of short characteristics. The code is explicitly photon-conserving in both space and time, which ensures an accurate tracking of ionization fronts, independent of the spatial and time resolution, even for grid cells which are optically thick to ionizing photons and time steps long compared to the ionization time of the atoms, with corresponding great gains in efficiency. The code has been tested against analytical solutions [17] and, in direct comparison with other radiative transfer methods, on a standardized set of benchmark problems [18]. C²Ray has also been used in the first, 3D radiation-hydrodynamical simulations of an H II region in a turbulent molecular cloud [19]. While our basic methodology remains essentially as described in [17], our C²Ray code is now parallelized for distributed-memory machines [14].

With CubeP³M, we simulated the Λ CDM universe with 1728^3 and 3072^3 N -body particles of mass $5 \times 10^6 M_\odot$, in comoving box sizes of 91 Mpc and 163 Mpc, respectively. At 29 billion particles, the latter is the largest N -body simulation of the formation of early cosmological structure to date. This mass resolution allows us to resolve all halos above $10^8 M_\odot$, roughly the minimum mass of halos which can radiatively cool by hydrogen atomic-line excitation and efficiently form stars. These halos are separated into halos above the Jeans mass of the ionized IGM ($\sim 10^9 M_\odot$), which are not affected by reionization, and lower-mass halos, whose star formation is suppressed if the halo formed inside an intergalactic H II region.

Figure 1 (a) shows the halo mass functions at $z = 6$ for three of our N -body simulations. These N -body simulations, i.e. the halo catalogues and density field, are the basis for our C²Ray radiative transfer simulations of reionization. All halos are assumed to host galaxies, and thus, ionizing sources, unless they form inside an H II region with a mass below the threshold for “Jeans-mass filtering”. To each galaxy, we assign an ionizing photon luminosity proportional to the halo mass, with an efficiency, f_γ , which gives

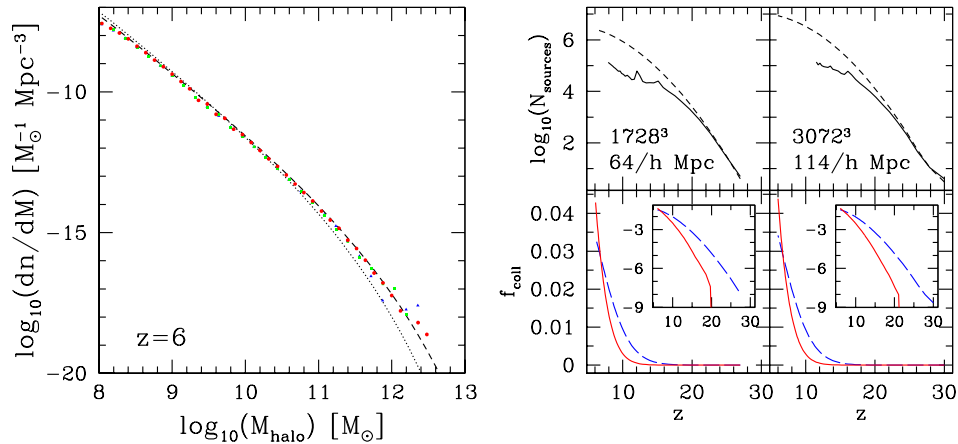


FIGURE 1. (a)(left) Halo mass functions at $z = 6$ from N -body simulations of Λ CDM with box sizes 91 Mpc (blue triangles), 103 Mpc (green squares) and 163 Mpc (red circles). The three mass functions agree with each other, except for the largest halos, which are subject to cosmic variance for the smaller volume simulations. The lines show the predicted mass functions based on the well-known analytical models of Press-Schechter ([20]; dotted) and Sheth-Tormen ([21]; dashed). (b) (right) (top panels) Total number of halos (dashed) and number of active sources (i.e. total number minus the suppressed ones; solid); and (bottom panels) collapsed mass fraction in high-mass (red, solid) and low-mass (i.e. suppressible) sources (blue, dashed) (insets show the same in log scale) vs. cosmic redshift for simulations f100_250S_91Mpc (left) and f50_250S_163Mpc (right).

the number of photons emitted per atom over the lifetime of the sources (here assumed to be 17.6 and 11.5 Myr for our 91 Mpc and 163 Mpc simulations, respectively). The simulations are denoted f100_250S_91Mpc_432 and f50_250S_163Mpc_384, where the first two numbers are the values of f_γ for the high- and low-mass sources, respectively, “S” indicates that source suppression due to Jeans-mass filtering was included, the third is the box size and the last is the radiative transfer grid resolution per dimension.

Figure 1(b) shows the evolution of the total source numbers, active source numbers and the fractions of the mean mass density collapsed into the two types of sources, those too massive to be suppressed by reionization and those which are sources only if they form in a neutral patch of the IGM. Figure 2 (and accompanying animation¹) shows images of the gas density field and (active) source halos overlaid with the ionized fraction field derived from our radiative transfer simulations. These indicate the complex, evolving geometry and topology of the network of ionized bubbles and neutral patches, which we must calculate in detail in order to make predictions of the fluctuating 21-cm background from this EOR.

The evolution of the mean ionized fractions of the IGM, mass-weighted (x_m) and volume weighted (x_v), is shown in Figure 3, including a comparison with those from our previous simulations of “self-regulated” reionization in a smaller box (50 Mpc), described in [13], and those from our previous large-box (143 Mpc) simulations with halo

¹ This Quicktime movie is playable with MPlayer and some Windows Media Players.

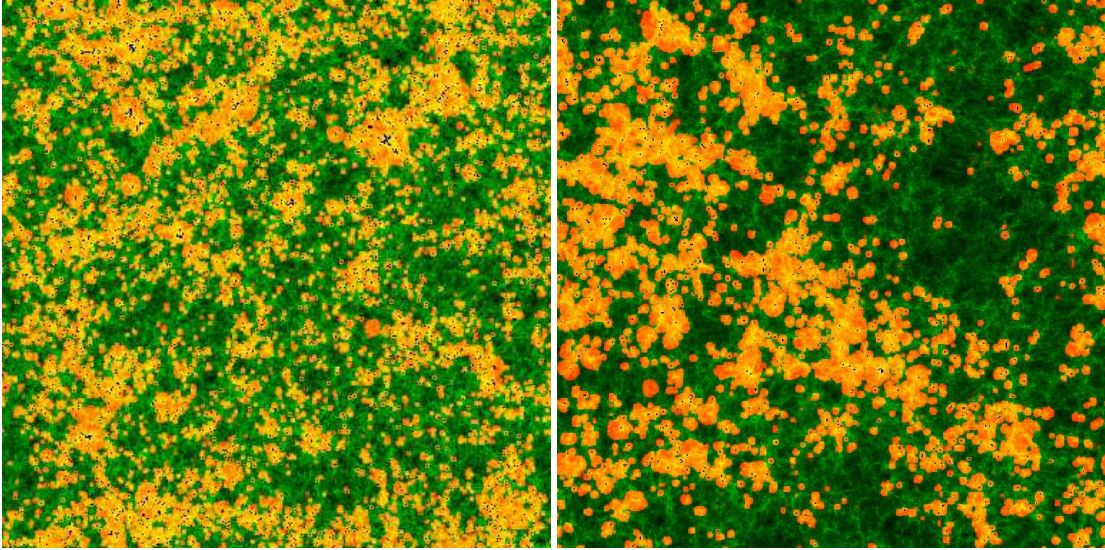


FIGURE 2. Spatial slices of the ionized and neutral gas density from our radiative transfer simulations (a)(left) boxsize 163 Mpc at redshift $z = 11.6$ and (b)(right) boxsize 91 Mpc at $z = 11.9$, both at box-averaged ionized fraction by mass $x_m = 0.30$. Shown are the density field (green) overlaid with the ionized fraction (red/orange/yellow) and the cells containing sources (dark/blue). There is a good agreement between the two simulations in the typical sizes of the locally-percolated ionization bubbles. [A “Quicktime” animation of the simulation on the right is included here.]

masses above $10^9 M_\odot$ only (i.e. no suppressible, low-mass halos) [12]. In all cases, reionization proceeds “inside-out” – i.e. halos form in high-density regions, clustered around density peaks and ionize these environments first, so $x_m > x_v$. For the new, self-regulated case shown there, $x_m = 0.1, 0.5$, and 0.99 at $z = 13.9, 10.7$, and 7.9 , respectively. As described in [13], the effect of including the lower-mass (suppressible) halos is to enable reionization to start earlier, since the low-mass halos are more abundant earlier. The end of reionization is not significantly affected, however, since it is dominated by the exponential rise of the abundance of the higher-mass halos, which are unaffected by Jeans-mass filtering of the IGM, while the abundance of low-mass halo sources saturates as the ionized volume grows.

Predictions of the fluctuating 21-cm brightness temperature, δT_b , from our 91 Mpc box ($\Delta\theta_{box} \sim 35'$ at $z \sim 8$) simulations are shown in Figure 4, which maps the sky along the line of sight in position - redshift (i.e. angle-frequency) space. The rms fluctuations shown in Figures 5(a) and (b) for this case and the 163 box simulations, too, vary with frequency as the ionization and density fluctuations evolve in redshift. There is a broad but distinct peak in the frequency range $\Delta\nu \approx 120 - 140$ Hz (i.e. $x_m \approx 0.5 - 0.8$). Figure 5(c) also shows the 2-D angular power spectrum of δT_b when $x_m = 0.3$, which peaks at $l \approx 3 - 4 \times 10^4$. Qualitatively similar features have been seen before from EOR simulations, but these are the first simulations which are *not only of volumes large enough* to make statistically reliable predictions, *but also of mass-resolution high enough* to take explicit account of the self-regulated nature of reionization.

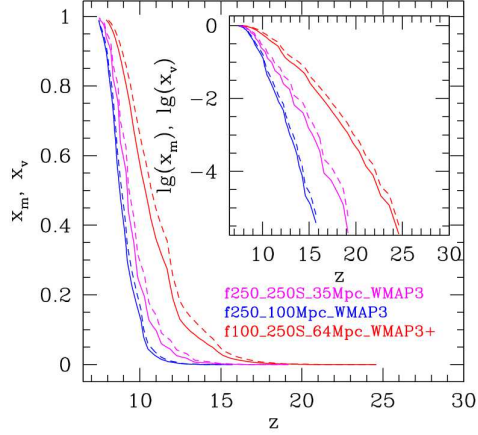


FIGURE 3. Mean ionized fractions, x_m (mass-weighted; dashed) and x_v (volume-weighted; solid) vs. redshift for three simulations: new simulations of box size 91 Mpc (f100_250S_64Mpc_WMAP3+; red; N.B. size label “64” here means “64/ h ”, where $h = 0.7$); previous “self-regulated reionization” simulations of box size 50 Mpc (f250_250S_35Mpc_WMAP3; magenta) from [13]; previous large-volume simulations *without* low-mass halos, of box size 143 Mpc (f250_100Mpc_WMAP3; blue) from [12].

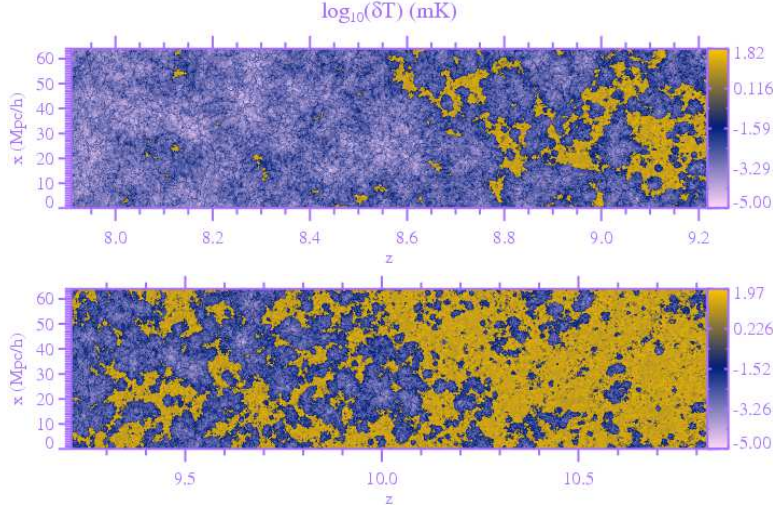


FIGURE 4. Sky map of 21-cm brightness temperature fluctuations, $\delta T_b \equiv (T_b - T_{\text{CMB}})/T_{\text{CMB}}$, along LOS, for 91 Mpc box reionization simulations, at observed frequencies $\nu_{\text{obs}}(\text{MHz}) = 142[(1+z)/10]$.

ACKNOWLEDGMENTS

This work was supported in part by NSF grant AST 0708176, NASA grants NNX07AH09G and NNG04G177G, Chandra grant SAO TM8-9009X, Swiss National Science Foundation grant 200021-116696/1, Swedish Research Council grant 60336701, and Texas Advanced Computing Center (TACC) computer allocation.

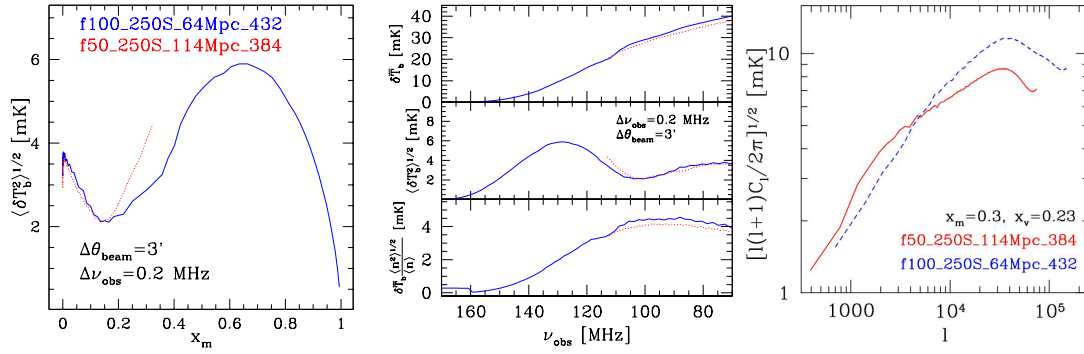


FIGURE 5. 21-cm brightness temperature fluctuations (a) (left) rms fluctuations $\langle \delta T_b^2 \rangle^{1/2}$ [mK] versus mean ionized fraction x_m , for 91 Mpc (solid) and 163 Mpc (dotted) simulations, if observed with a beamwidth $\Delta\theta_{\text{beam}} = 3'$ and bandwidth $\Delta\nu_{\text{obs}} = 0.2$ MHz; (b) (middle) mean differential brightness temperature $\overline{\delta T_b}$ [mK] (top) and rms $\langle \delta T_b^2 \rangle^{1/2}$ [mK] (middle) versus observed frequency, and, for comparison, $\overline{\delta T_b} \langle n^2 \rangle^{1/2} / \langle n \rangle$, to show that signal is enhanced relative to matter fluctuations, by reionization patchiness, and evolves differently; (c) (right) 2-D angular power spectrum of δT_b vs. l , for epoch at which $x_m = 0.3$.

REFERENCES

1. S. R. Furlanetto, S. P. Oh, and F. H. Briggs, *Phys. Reports* **433**, 181–301 (2006).
2. R. Barkana, *Science* **313**, 931–934 (2006).
3. B. Ciardi, and A. Ferrara, *Space Science Reviews* **116**, 625–705 (2005).
4. P. R. Shapiro, M. L. Giroux, and A. Babul, *ApJ* **427**, 25–50 (1994).
5. I. T. Iliev, G. Mellema, U.-L. Pen, H. Merz, P. R. Shapiro, and M. A. Alvarez, *MNRAS* **369**, 1625–1638 (2006).
6. O. Zahn, A. Lidz, M. McQuinn, S. Dutta, L. Hernquist, M. Zaldarriaga, and S. R. Furlanetto, *ApJ* **654**, 12–26 (2007).
7. K. Kohler, N. Y. Gnedin, and A. J. S. Hamilton, *ApJ* **657**, 15–29 (2007).
8. H. Trac, and R. Cen, *ApJ* **671**, 1–13 (2007).
9. G. Mellema, I. T. Iliev, U.-L. Pen, and P. R. Shapiro, *MNRAS* **372**, 679–692 (2006).
10. I. T. Iliev, U.-L. Pen, J. R. Bond, G. Mellema, and P. R. Shapiro, *ApJ* **660**, 933–944 (2007).
11. I. T. Iliev, P. R. Shapiro, P. McDonald, G. Mellema, and U.-L. Pen, *ArXiv e-prints 0711.2994* (2007).
12. I. T. Iliev, G. Mellema, U.-L. Pen, J. R. Bond, and P. R. Shapiro, *MNRAS* **384**, 863–874 (2008).
13. I. T. Iliev, G. Mellema, P. R. Shapiro, and U.-L. Pen, *MNRAS* **376**, 534–548 (2007).
14. I. T. Iliev, G. Mellema, H. Merz, P. R. Shapiro, and U.-L. Pen, *TeraGrid08* (2008), in press.
15. R. W. Hockney, and J. W. Eastwood, *Computer simulation using particles*, Bristol: Hilger, 1988.
16. H. Merz, U.-L. Pen, and H. Trac, *New Astronomy* **10**, 393–407 (2005).
17. G. Mellema, I. T. Iliev, M. A. Alvarez, and P. R. Shapiro, *New Astronomy* **11**, 374 (2006).
18. I. T. Iliev, B. Ciardi, M. A. Alvarez, A. Maselli, A. Ferrara, N. Y. Gnedin, G. Mellema, T. Nakamoto, M. L. Norman, A. O. Razoumov, E.-J. Rijkhorst, J. Ritzerveld, P. R. Shapiro, H. Susa, M. Umemura, and D. J. Whalen, *MNRAS* **371**, 1057–1086 (2006).
19. G. Mellema, S. J. Arthur, W. J. Henney, I. T. Iliev, and P. R. Shapiro, *ApJ* **647**, 397–403 (2006).
20. W. H. Press, and P. Schechter, *ApJ* **187**, 425–438 (1974).
21. R. K. Sheth, and G. Tormen, *MNRAS* **329**, 61–75 (2002).